◎ 논 문
◎ Original Paper

DOI: http://dx.doi.org/10.5293/kfma.2014.17.5.060
ISSN (Print): 2287-9706

Performance and Cavitation Analysis on Tidal Current Turbine for Low Water Level Channel

Chengcheng Chen* · Young-Do Choi**†

Key Words : Tidal current turbine(조류터빈), Blade design(블레이드 설계), Hydrofoil(하이드로포일), Performance(성능), Cavitation (캐비테이션)

ABSTRACT

Most tidal current turbine designs are focused on medium and large scale for deep sea, less attention is paid in low water level channel, such as the region around the islands and costal sea. This study is to develop a horizontal axis tidal current turbine rotor blade which is applicable to low water level island region in southwest coastal region of Korea. In this study, the hydrofoil NACA63-415 and NACA63-817 are both adopted to analyze. The blade using NACA63-817 showed the higher maximum power coefficient and good performance at small TSR (Tip Speed Ratio), which gives the blade more advantages in operating at lower water level channel, where is characterized by the fast-flowing water. The cavitation pattern of hydrofoil is predicted by the CFD analysis and verified that the NACA63-817 is the appropriate hydrofoil in the test site of tidal current resource and the hydrofoil showed considerable performance in avoiding cavitation.

1. Introduction

There are over a thousand islands in the southwest coast of Korea. Although the population of the islands being decreases annually, the power consumption in the region annually increases due to the growth of the convenient facilities.[1]

Under the economic growth circumstances, small islands that face difficulties in connecting to electric power network, and seek to expend their independent diesel power plants, so more power generations are required.

Less tidal current turbine system is applied to the southwest coast of Korea island region, as the sea area near the islands are shallow, the middle or large scale tidal can not be set up. But the shallow sea area is rich in current tidal energy and produces reliable, predictable and continuous energy source throughout the year.

The higher density of water relative to air (water is about 800 times of the density of air) means that a single generator can provide significant power at low tidal flow velocities compared with similar wind turbines. However, it is accompanied with high possible cavitation, which will sharp decreases of performance and serve life.[2-7]

Therefore, 4 hydrofoils are compared to achieve a blade with low possible of the cavitation occurrence, on the premise of high power coefficient

* Graduate School, Department of Mechanical Engineering, Mokpo National University, Mokpo
** Department of Mechanical Engineering, Institute of New and Renewable Energy Technology Research, Mokpo National University, Mokpo
† 교신저자(Corresponding Author), E-mail : ydchoi@mokpo.ac.kr

2013 한국유체기계학회 학술대회 발표 논문, 2013년 11월 27-29일, 제주
The KSFM Journal of Fluid Machinery: Vol. 17, No. 5, October, 2014, pp.60~66(Received 5 Dec. 2013; accepted for publication 7 Apr. 2014)

2. Site Survey

Fig. 1 shows the annual energy density in the south-western region. Yang et al.[8] assessed the tidal current energy in South Jeolla Province and suggests some candidate locations for tidal current power plants. Byun et al.[9] carried out a study to estimate the prospective tidal current energy resources off the south and west coasts of Korea. It is found that off the coast of Jeonnam Province include the greatest concentration of high energy density sites, including: Uldolmok, Geocha waterway, Changjuk waterway, Maenggol waterway and Hoenggan waterway.

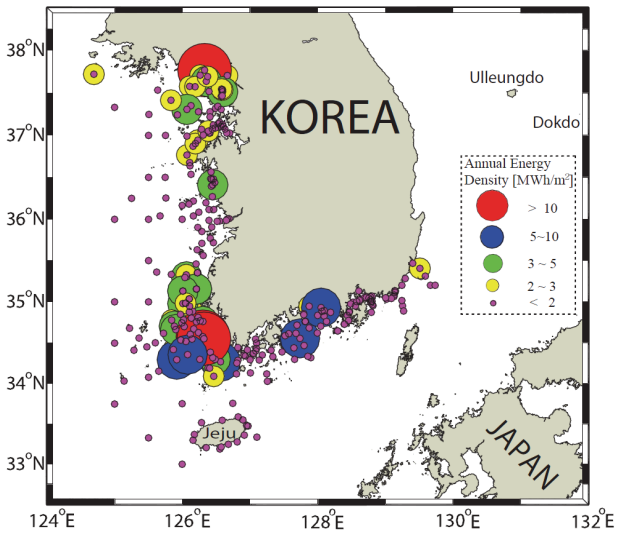

Fig. 1 Tidal energy densities of South Korea

Fig. 1 shows that the high annual tidal average energy densities are mainly found in waterways characterized by narrow widths, since this landform leads to strong, rectilinear tidal current flows[9]. Therefore, it can be considered that a turbine deployment in the Uldolmok Strait between Jindo and Haeman.

Fig. 2(a) presents the channel landform condition clearly. The channel is an excellent likeness to a pipe, no sharply extruding ledge on the channel bed, and the smooth bed focus on the range of depth 20m~30m[10].

Due to narrow widths, strong tidal current is produced in Uldolmok: the maximum current speeds and no significant neap reduction as shown in Fig. 2(b). The observed strong currents result from the highly dominant nature narrow landform.

3. Tidal Current Turbine Design

3.1. Hydrodynamic characteristic of 4 hydrofoils

The hydrodynamic characteristics are very important in the selection of a high performance hydrofoil. The performance of the turbine depends on three very important parameters: the lift coefficient (C_L), lift to drag ratio (C_L/C_D), and the Reynolds number (Re). At the design point, where the tidal current velocity is 2.5 m/s, the Reynolds number is about 2 million.

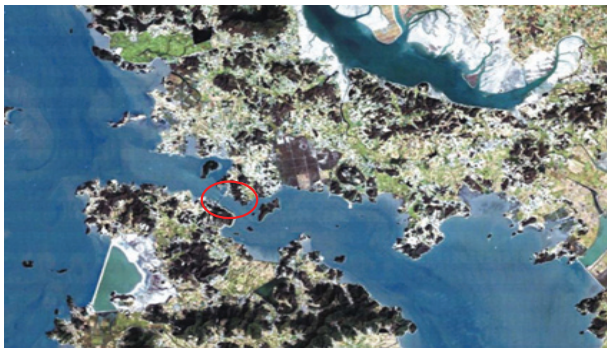

(a)

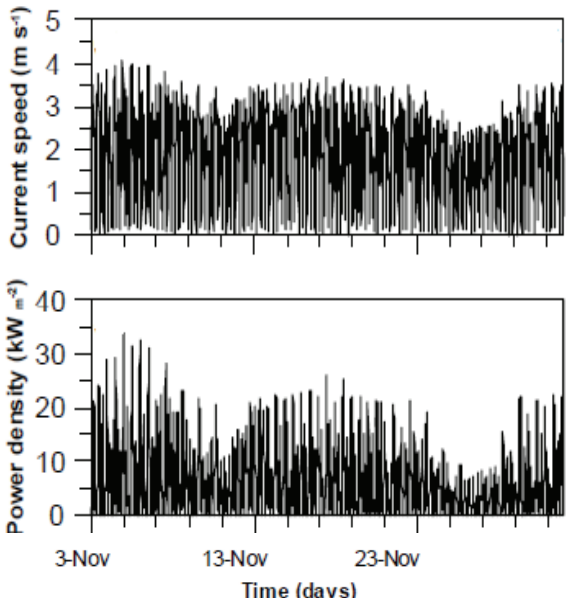

(b)

Fig. 2 (a) Location of Uldomok water channel and (b) Tidal current condition at the region

Fig. 3 shows adopted NACA63-series hydrofoils which are widely known for its good aerodynamic characteristic and less sensitive to leading edge roughness.

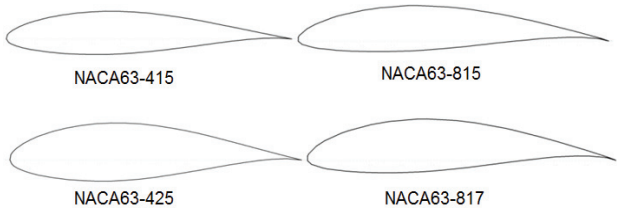

Fig. 3 Adopted NACA63-series hydrofoils for performance comparison

In the hydrodynamic characteristics analysis using X-foil,[11] the NACA63-817, NACA63-815, NACA63-425, NACA63-415 are adopted as shown in Fig. 4. Though NACA63-415 provides a relatively large range of high lift to drag coefficient, NACA63-817 showed its relatively higher lift coefficient among the hydrofoils.

3.2. Cavitation analysis

A big challenge in the design of blade for tidal current turbine is to avoid cavitation and still obtain an acceptably high power coefficient. The possibility of cavitation occurrence will rise with the increase of the inflow velocity. The blade which is designed for lower water level channel needs more attention of predicting cavitation, as the flow is characterized by the fast-flowing water.

Cavitation inception is assumed to occur when the local pressure on the blade surface falls to, or below, that of the vapour pressure of the fluid. Cavitation number and pressure coefficient are introduced to predict the possibility of cavitation occurrence[12]. The cavitation number and pressure coefficient are defined as Eq.(1) and Eq.(2):

$$\sigma = \frac{(P_{AT} + \rho g h - P_V)}{0.5\rho V^2} \quad (1)$$

$$C_P = \frac{(P_L - P_O)}{0.5\rho V^2} \quad (2)$$

Where P_{AT} is the atmospheric pressure, P_V is the vapour pressure, P_O is the free stream pressure, P_L is the local pressure around the hydrofoil, ρ is the density of fluid, h is the minimum depth between the blade tip and the water surface, V is the inflow velocity.

Cavitation can be predicted from the pressure distribution since the cavitation will occur in the situation of the negative pressure coefficient $-C_P \geq \sigma$, or when $P_L \leq P_V$.

To investigate the cavitation occurrence of NACA63-415 and NACA63-817, which have relatively wider range of high lift to drag coefficient and relatively higher lift coefficient each other, the negative pressure coefficient is compared with the cavitation number as shown in Fig. 5.

In case of NACA63-415 hydrofoil, the cavitation number is higher than negative pressure coefficient, which means that NACA63-415 hydrofoil have the possibility of cavitation occurrence. However, in case of NACA63-817 hydrofoil showed lower pressure coefficient than cavitation number.

The further prediction of cavitation is carried out by the air volume friction distribution around the hydrofoil.

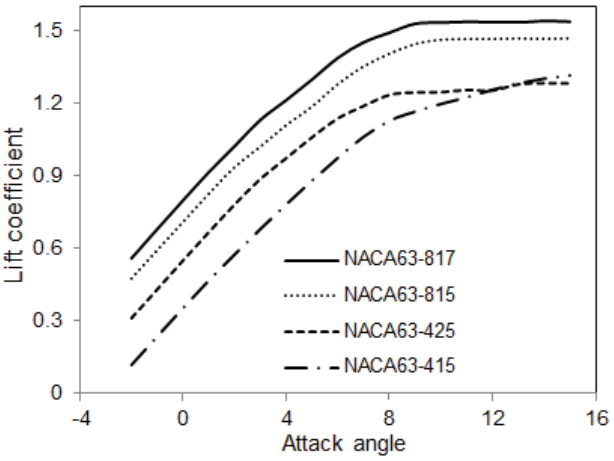

(a)

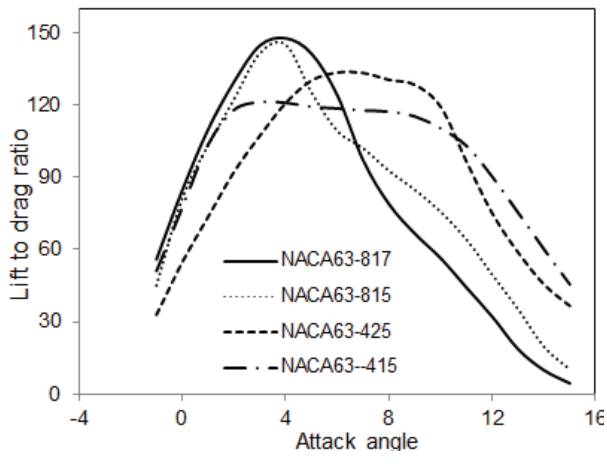

(b)

Fig. 4 (a) Lift coefficient of 4 hydrofoils at Re=2×10^6; (b) Lift to drag ratio of 4 hydrofoils at Re=2×10^6

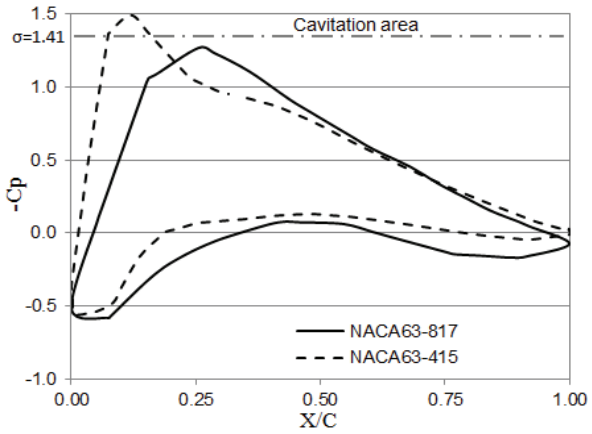

Fig. 5 Pressure coefficient and cavitation number relationship

From Fig. 6 it is also seen that air particles begins to form considerably near the trailing edge on the suction and pressure sides of the NACA63-415 hydrofoil at time steps of 0.005s. With the time going, air particles become stable and level off on the blade suction surface. Fig. 7 showed the air particles around the NACA63-817 hydrofoil at the beginning but some small air particles emerges, and then, it is quickly suppressed after the time step of 0.05s. Therefore, the NACA63-817 hydrofoil can be considered safe to be used for tidal current turbine design.

Table 1 Blade Design Parameters

Design parameter	Values
P_{rated}: Prated: rated power	100 KW
C_P: Estimated power coefficient	0.46
V_O: Rated current velocity	2.5 m/s
ρ: Sea water density	1025 kg/m3
D: Diameter of blade	6.2 m
ω: rated rotational speed	45 rpm
λ_D: Design tip speed ratio	5.8
λ_O: Optimized tip speed ratio	6

3.3. Blade design by BEMT

Table 1 shows the blade design parameters, which are determined by the actual operation condition of horizontal axis tidal current turbine(HATCT). Fig. 8 shows the chord length and twist angle adopted for the design of a 3-pieces rotor blade.

In addition, Blade Element Momentum Theory (BEMT) is adopted to optimize the design for a rotor blade with the consideration of tidal current conditions at installation site. Fig. 9 shows the shape of designed rotor blade model and radius ratios for the investigation of cavitation occurrence at the locations.

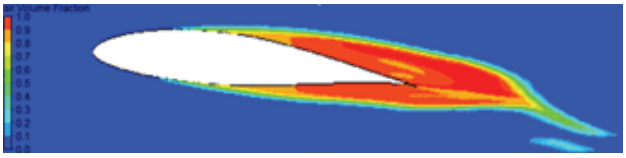

0.005s

0.05s

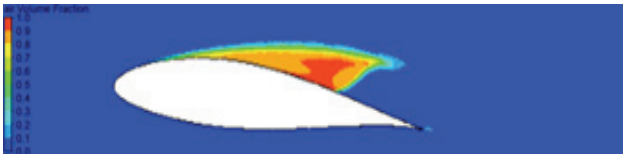

0.1s

Fig. 6 Time steps cavitation characteristic on NACA63-415

0.005s

0.05s

0.1s

Fig. 7 Time steps cavitation characteristic on NACA63-817

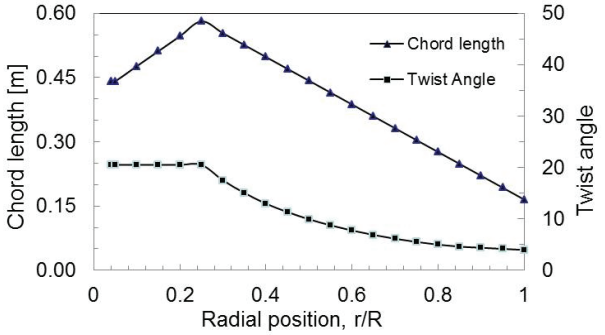

Fig. 8 Chord length and twist angle of rotor blade

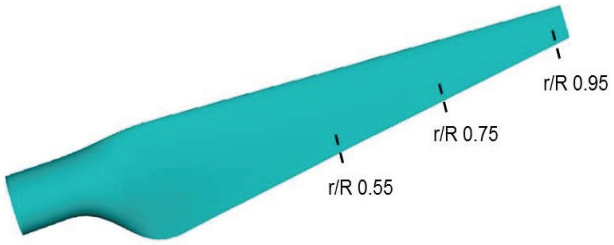

Fig. 9 Shape of designed rotor blade model

4. Numerical methods

One blade and one third of the flow field is analyzed as shown in Fig. 10. Considering the computational time, the total numbers of numerical grids are about 5 million nodes. Hexahedral structural grids are used to increase the convergence of the calculation. To predict the torque, pressure and velocity streamline occurring on the blade surface, O-grid is used for the blade surface mesh.

Table 2 shows summary of boundary condition for the numerical analysis. ANSYS CFX[13] is used as a solver to conduct the numerical analysis. For a turbulence model, the Shear Stress Transport *(SST)* model is used, which has been well known to estimate both separation and vortex occurring on the wall of a complicated blade shape, as well as to describe the main fluid flow.

The general connect is setting as the frozen rotor condition between the rotational area and the fixed area in the flow field. The pressure outlet boundary condition is applied at the exit of calculation domain.

5. Results and Discussion

5.1. Power coefficient

The power coefficient is given by Eq. (3), where P_T is the product of torque and angular velocity, and the denominator represents the power available from the tidal current. The two types of rotor blade, NACA63-817 and NACA63-415, are compared for the power coefficient(C_{Power}) each other.

$$C_{Power} = \frac{P_T}{0.5\rho v^3} \tag{3}$$

Fig. 11 shows that the maximum power coefficient of NACA63-817 blade is 0.478 at TSR 6, which is higher than maximum power coefficient 0.467 of NACA63-415 at TSR 7. Therefore, the blade using NACA 63-817 has the advantage of output power at low TSR, which results in relatively more output power at site condition of high tidal current speed.

5.2. Pressure distribution on the rotor blade surface

In order to examine the hydrodynamic characteristics of the HATCT rotor blade using NACA63-817 hydrofoil by CFD analysis, the value of pressure coefficient (Cp) surrounding the blade pressure and suction surfaces is compared quantitatively as shown in Fig. 12, according to the blade radial local radius ratio. As shown in Fig. 12, X/C on the abscissa in the figures presents dimensionless length; X is the length from the leading edge to the trailing edge of the hydrofoil; and C is the chord length.

Table 2 Boundary condition

Condition	Values
Turbulence model	SST
Mesh connect	GGI
Inlet velocity	1.6-5 m/s (TSR 3-9)
Outlet static pressure	0 Pa
Rotation speed	45 min^{-1}
Blade surface	No slip wall

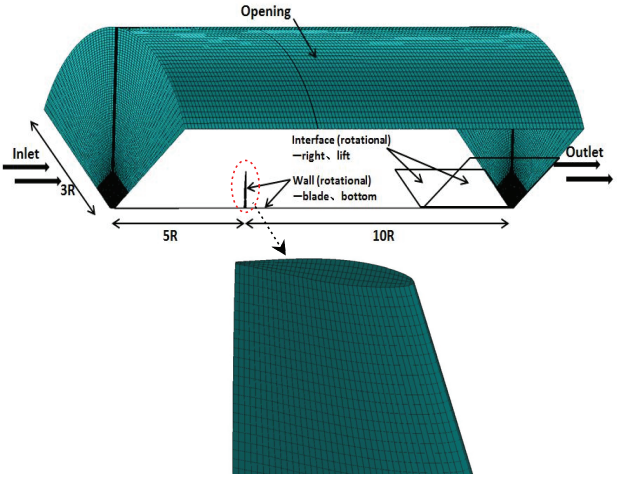

Fig. 10 Numerical grid and boundary conditions for computational analysis

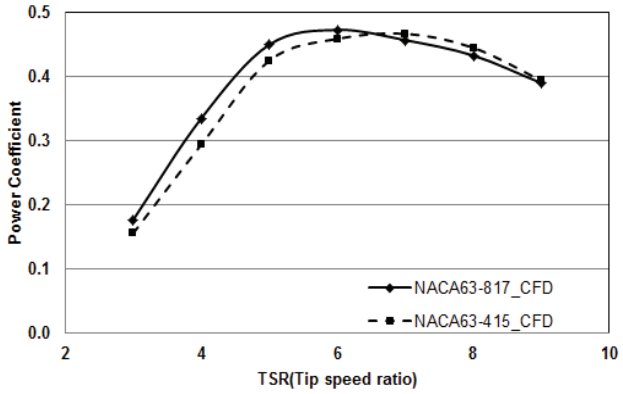

Fig. 11 Power coefficient curve for two rotor blade

The maximum area of pressure difference between the pressure and suction surfaces is observed at the location of 75% and slightly less at 95% of the local radius to the tip.

Moreover, Fig. 12 shows the result of comparison of cavitation occurrence possibility test using the designed rotor blade by NACA63-817 hydrofoil. As explained in Fig. 5, if the value of $-C_p$ rises over the line of cavitation number σ, possibility of cavitation occurrence is very high. However, The result reveals that $-C_p$ values at the 3 radial locations of the blade are below the cavitation number line. Therefore, it is conjectured that turbine blade has a superior cavitation performance.

5.3. Streamlines on the rotor blade surface

Fig. 13 presents the streamline distribution on the blade surface for TSR ranges 3~9 of the rotor blade by NACA63-817 hydrofoil. It can be observed that streamlines at lower TSR showed a stronger radial flow formed near the root suction side. Besides, the streamlines at TSR 3 showed radial flow formed across more than 75% of the radial location starting from root. This radial flow creates an irregular flow on the blade surface and affects the hydrodynamic characteristics of the turbine by decreasing the output power and power coefficient.

The streamlines at TSR 6 and TSR 9 showed relatively uniform flow to the rotational direction except for the local region near the hub, which means relatively higher output power than that at TSR 3. However, in case of TSR 9, a larger TSR means a lower current velocity, which results in lower torque on blade as well as lower power coefficient of the turbine.

Therefore, in order for the turbine to run at excellent power coefficient, TSR should be in the range of 5~7 in consideration with the results of power coefficient and flow characteristics in Figs. 11 and 13.

6. Conclusion

The performance and cavitation analysis on a horizontal axis tidal current turbine are presented for low water level channel. The Uldolmok Strait between Jindo and Haeman is selected as a suitable location for the turbine blade. By comparing several common hydrofoils, the blade using NACA63-817 showed a higher maximum power coefficient, and good performance

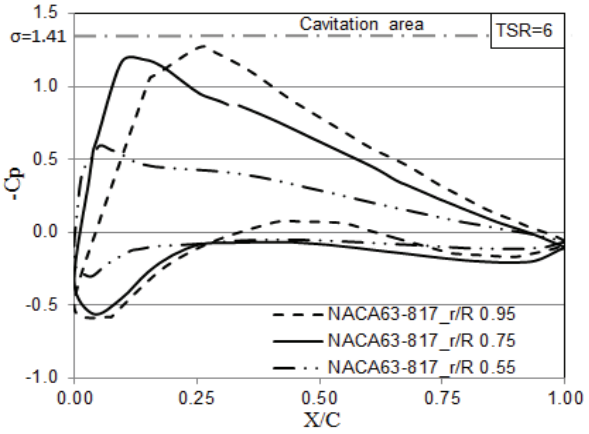

Fig. 12 Pressure coefficient on the blade surface for different blades radius

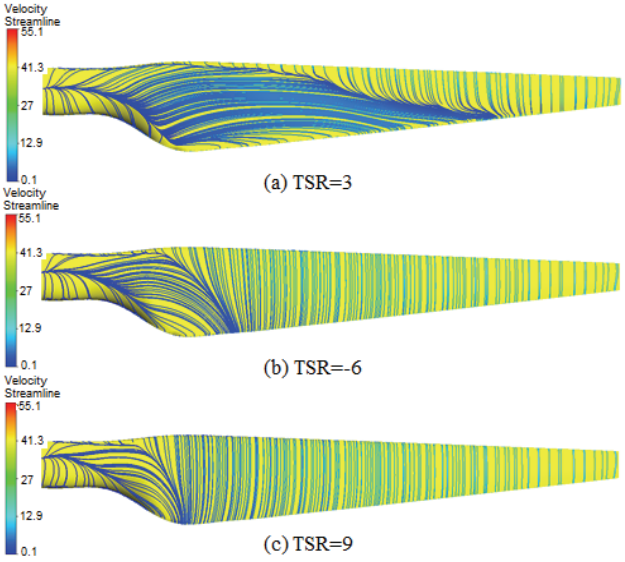

Fig. 13 Streamline on the blade surface from TSR 3-9

at small TSR gives more advantages to the blade in operating at lower water level channel, where is characterized by the fast-flowing water. The cavitation pattern of hydrofoil is predicted by CFD analysis and verifies that the NACA63-817 is the appropriate hydrofoil in this design which showed considerable performance in avoiding cavitation.

References

(1) Lee, J. Y., Choi, N. J., Yoon, H. Y. and Choi Y. D., 2012, "Design and Flow Analysis on the 1kW Class Horizontal Axis Wind Turbine Rotor Blade for Use in Southwest islands Region," Journal of Fluid Machinery, Vol. 15, No. 3, pp. 5~11.

(2) Esteban, M. and Leary, D., 2012, "Current Developments and Future Prospects of Offshore Wind and Ocean Energy," Appl. Energy, Vol. 90, pp. 128~136.

(3) Ahmed, M. R., 2012, "Blade Sections for Wind Turbine and Tidal Current Turbine Applications-Current Status and Future Challenges," International Journal of Energy Research, Vol. 36, pp. 829~844.

(4) T. Burton, D. Sharpe, N. Jenkins, E. Bossanyi, Wind Energy Handbook, John Wiley & Sons, Ltd, pp.41~65.

(5) Nicholls-Lee, R. F., Turnock, S. R. and Boyd, S. W., 2013, "Application of Bend-Twist Couple Blades for Horizontal Axis Tidal Turbines," Renewable Energy, Vol. 50, pp. 541~550.

(6) Liu, D. M., Liu, S. H., Wu, Y. L. and Xu, H. Y., 2009, "Les Numerical Simulations of Cavitation Bubble Shedding on ALE 25 and ALE 15 Hydrofoils," Journal of Hydro dynamics, Vol. 21, No. 6, pp. 807~813.

(7) Arndt, R. E. A., 1981, "Cavitation in Fluid Machinery and Hydraulic Structures," Annu. Rev. Fluid Mech, Vol. 13, pp. 273~328.

(8) Yang, C. J. and Lee, Y. H., 2012, "An Overview of Tidal Current Energy in South Jeolla Province, Korea," Proceedings of Asian Wave and Tidal Conference Series. pp. 333~336.

(9) Byun, D. S., Hart, D.E. and Jeong, O. J., 2013. "Tidal Current Energy Resources off the South and West Coasts of Korea: Preliminary Observation-Derived Estimates," Energies 2013, pp. 567~573.

(10) LEE, K. S., 2006. "Tidal and Tidal Current Power Study in Korea," the East Asian Seas Congress 2009.

(11) MIT Aero & Astro, 2013, http://web.mit.edu/drela/Public/web/xfoil/.

(12) Batten, W. M. J., Bahaj, A. S., Molland, A. F., Chaplin, J. R., 2006. "Hydrodynamics of Marine Current Turbines," Journal of Renewable Energy, Vol. 31, pp. 249~256.

(13) ANSYS Inc, 2013, "ANSYS CFX Documentation" Ver. 14, http://www.ansys.com